Unveiling spin-dependent unoccupied electronic states of Co_2MnGe (Ga) film via Ge (Ga) $L_{2,3}$ absorption spectroscopy

T. Yoshikawa,[1,*] V. N. Antonov,[2,3] T. Kono,[1] M. Kakoki,[1] K. Sumida,[1,4,5] K. Miyamoto,[6] Y. Takeda,[5] Y. Saitoh,[5] K. Goto,[7] Y. Sakuraba,[7] K. Hono,[7] A. Ernst,[2,8] and A. Kimura[1,9,†]

[1]*Graduate School of Science, Hiroshima University, 1-3-1 Kagamiyama, Higashi-Hiroshima, Hiroshima 739-8526, Japan*
[2]*Max Planck Institute of Microstructure Physics, D-06120 Halle (Saale), Germany*
[3]*G.V. Kurdyumov Institute for Metal Physics of the N.A.S. of Ukraine, UA-03142 Kyiv, Ukraine*
[4]*Department of Physics, Tokyo Institute of Technology, Tokyo 152-8551, Japan*
[5]*Materials Sciences Research Center, Japan Atomic Energy Agency, Hyogo 679-5148, Japan*
[6]*Hiroshima Synchrotron Radiation Center, Hiroshima University, 2-313 Kagamiyama, Higashi-hiroshima 739-0046, Japan*
[7]*National Institute for Materials Science, Sengen 1-2-1, Tsukuba 305-0047, Japan*
[8]*Institute for Theoretical Physics, Johannes Kepler University, A-4040 Linz, Austria*
[9]*Graduate School of Advanced Science and Engineering, Hiroshima University, 1-3-1 Kagamiyama, Higashi-Hiroshima 739-8526, Japan*

(Received 24 May 2020; accepted 10 August 2020; published 26 August 2020)

X-ray absorption spectroscopy (XAS) and x-ray magnetic circular dichroism (XMCD) spectroscopy were applied at the Ge (Ga) $L_{2,3}$ edge to unravel the spin-resolved unoccupied electronic states of Co_2MnGe (Ga). Complicated spectral features were observed in both XAS and XMCD spectra. For their interpretation, we compared the experimental XAS and XMCD spectra with the calculated Ge (Ga) 4*s* and 4*d* orbital partial density of states. The comparison enabled a qualitative explanation of the XMCD spectra as the difference between the majority- and minority-spin unoccupied density of states summed over the 4*s* and 4*d* orbitals. Our finding provides a new approach to uncover the spin-split partial density of states above the Fermi level.

DOI: 10.1103/PhysRevB.102.064428

I. INTRODUCTION

Half-metallicity in magnetic materials is characterized by a metallic density of states and a semiconducting gap in the majority and minority-spin channels, resulting in a 100% spin polarization at the Fermi level (E_F). In such materials, the tunneling magnetoresistance (TMR) and giant magnetoresistance (GMR) are expected to rise substantially when used in spintronic devices [1]. First-principles calculations predict that some of the ferromagnetic Co-based full-Heusler alloys including Co_2MnGe and Co_2MnSi exhibit a half-metallic electronic structure [2–4]. Extremely high magnetoresistance (MR) ratios have been realized in TMR and GMR devices employing half-metallic Heusler electrodes [5–12]. However, a sharp drop in the MR ratio with elevating temperatures was detected, thereby impeding practical applications. To address this problem, the spin-dependent electronic structure both below and above E_F needs to be clarified experimentally. Photoemission spectroscopy is a powerful tool to observe occupied electronic states below E_F and therefore has been employed for half-metallic Heusler alloys in several previous studies [13–20]. However, there are only a few reports on spin-resolved unoccupied electronic states [21,22].

X-ray absorption spectroscopy (XAS) and x-ray magnetic dichroism (XMCD) spectroscopy provide core absorption spectra that enables these element-specific electronic structures to be examined [23]. Basically, the core absorption spectra excited with left and right circularly polarized x-ray radiation reflect the unoccupied partial density of states (PDOS) taking into consideration spin-dependent transition probabilities [24,25]. However, the core-hole created often causes a spin-dependent energy shift that arises from an attractive force between core hole and spin-polarized valence electrons. Furthermore, a strong localization of the Mn 3*d* electrons yields multiplet structures in the spectrum that considerably modify the initial unoccupied PDOS [26,27]. Several previous studies examined the extraction of the spin-dependent unoccupied PDOS through optical transitions from the spin-orbit splitting of the $2p_{3/2}$ or $2p_{1/2}$ core level into weakly localized Co 3*d* states [21,22]. The spin-dependent energy shift prevents an estimate of the correct value of the exchange splitting.

In this work, we focus on the $2p \rightarrow 4s$ or $4d$ dipole transitions of the nonmagnetic element Ge (Ga) in Co_2MnGe (Co_2MnGa). We expect that the core-hole effect is small because of the itinerant character of the Ge- (Ga) derived electrons and does not depend on the spin orientations. Because the exchange-split states of *d* electrons from a transition metal may be copied to the Ge (Ga) PDOS through hybridization, it is possible to uncover the spin-dependent unoccupied electronic states and estimate the magnitude of the exchange splitting in the system.

*tomoki-ysk@hiroshima-u.ac.jp
†akiok@hiroshima-u.ac.jp

II. EXPERIMENTAL AND COMPUTATIONAL DETAILS

Following the ultrahigh vacuum magnetron sputtering method, thin-film samples of Co_2MnGe (Ga) were grown at National Institute for Materials Science. The 30-nm-thick Co_2MnGe (Ga) films were grown through Ar^+ ion sputtering of their sintered alloy target onto a MgO substrate with buffer layers of Cr (10 nm) and Ag (100 nm) on the substrate to reconcile a lattice mismatch between substrate and ferromagnetic layer and thus suppress surface roughness. The Co_2MnGe (Ga) layer was annealed at 550°C to induce high atomic ordering. Finally, these samples were covered with Al (1 nm) to prevent further surface oxidation. X-ray diffractometry confirmed the existence of an $L2_1$-ordered phase in both Co_2MnGe and Co_2MnGa.

The XAS/XMCD experiment was performed at the twin helical undulator beamline of SPring-8 BL23SU. The total electron yield method was employed whereby fast switching of the x-ray helicity at 1 Hz enabled data acquisition even of weak signals such as from Ge (Ga) $L_{2,3}$ edge XMCD with an excellent signal-to-noise ratio [28]. The measurements were performed at 40 K.

The applied magnetic field was set to ±8 T. In the measurement, both the incident photon spin and the magnetization were oriented perpendicular to the sample surface. The XMCD spectrum reveals the difference $\mu_- - \mu_+$, where μ_+ and μ_- represent the absorption intensity with the magnetization directed parallel and antiparallel, respectively, to the photon spin.

We note that the escape depth of total electron yield XAS/XMCD would be around 2–3 nm [29]. Although it is not sufficiently long, we consider that the experimental XAS/XMCD spectra represent mostly bulk electronic states, which is supported by our recent photoemission experiment with soft x-ray synchrotron radiation [20] with exactly the same sample capped by 1-nm-thick Al, where most of the experimental results were well explained by the calculated bulk electronic structure.

The first-principles density-functional calculations were performed using the program WIEN2k [30] and a fully relativistic linear muffin-tin orbital (LMTO) method [31,32]. We used the spin-polarized generalized gradient approximation (GGA) as an approximation [33]. We adopted the experimental lattice constants $a = b = c = 5.753$ Å and $a = b = c = 5.767$ Å for Co_2MnGe and Co_2MnGa, respectively [34]. The XAS and XMCD spectra were computed based on Fermi's golden rule (see below) using the method described in Refs. [35–38].

III. RESULTS AND DISCUSSION

First, from the Ge $L_{2,3}$ edge XAS (XMCD) spectrum of Co_2MnGe [Fig. 1(a), upper (lower) panel], we see that the XAS intensity sharply rises at 1213.5 eV, corresponding to the onset of Ge L_3 absorption. There are two shoulders (A_3, B_3) and two peaks (C_3, D_3) in the L_3 absorption region. The size of the spin-orbit splitting (∼31 eV) between the Ge $2p_{3/2}$ and $2p_{1/2}$ edges indicates that the L_2 absorption edge starts from around 1245 eV, and four characteristic features then follow (A_2, B_2, C_2, D_2). The XMCD spectrum shows some

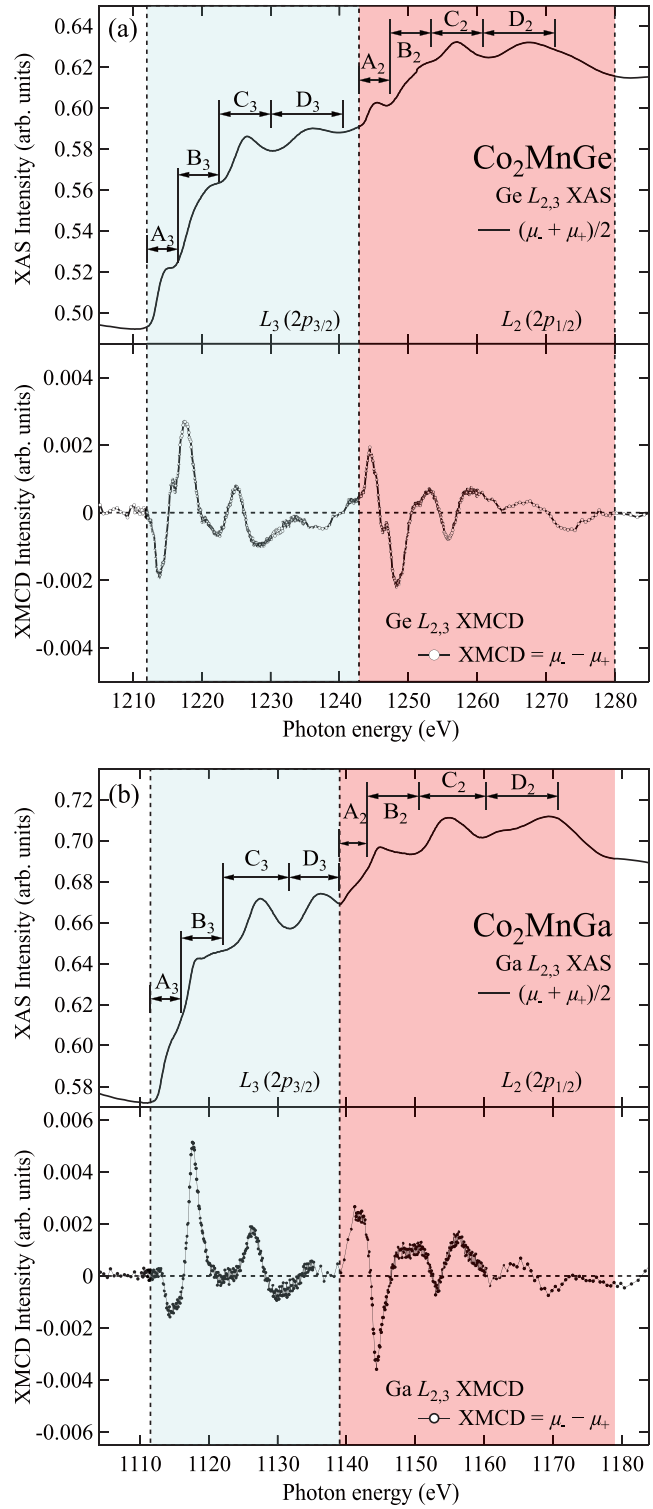

FIG. 1. $L_{2,3}$ XAS (upper) and XMCD (lower) spectra of (a) the Ge site of Co_2MnGe and (b) the Ga site of Co_2MnGa.

oscillating features starting with negative intensity at the L_3 edge, exhibiting a peak where the XAS intensity rises or falls. Its significance is that the XMCD follows the derivative of the XAS spectrum. We note that reversing the magnetic field also reverses the sign of the XMCD spectrum at the $L_{2,3}$ absorption edge, signifying that the observed features are essential. The

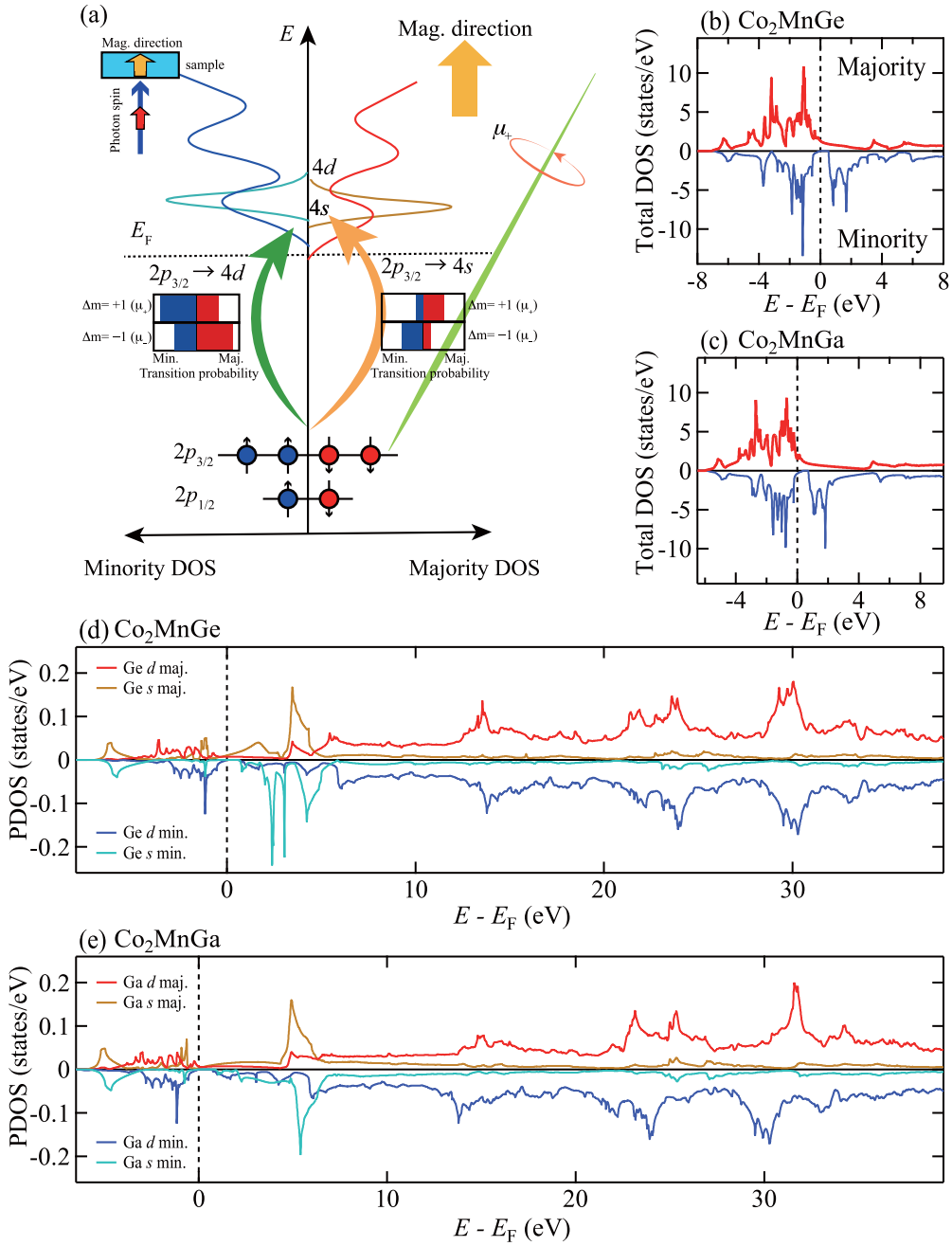

FIG. 2. (a) Schematic XMCD considering the transition probability for μ_+. [(b) and (c)] Calculated spin-dependent total DOS, and [(d) and (e)] the Ge and Ga PDOS for orbitals 4s and 4d in the extended energy range for Co_2MnGe and Co_2MnGa, respectively.

Ga $L_{2,3}$ XAS and XMCD spectra of Co_2MnGa [Fig. 1(b)] are similar to those at the Ge $L_{2,3}$ edge of Co_2MnGe in terms of their shapes. However, some differences are present in the XMCD spectra. The position of the largest positive peak in the experimental XMCD spectrum of Ga is higher by 0.8 eV than that of Ge with respect to the absorption edge (we discuss this point later). We also find that the first negative XMCD peak just above the absorption edge is wider for Co_2MnGa than that for Co_2MnGe. These Ge and Ga $L_{2,3}$ XAS and XMCD spectra are considered to originate from optical transitions $2p \rightarrow 4d$ and/or $2p \rightarrow 4s$, taking into account the dipole selection rule; see schematic in Fig. 2(a). Therefore, the observed XAS spectrum should reflect the Ge and Ga $4d/4s$ PDOS.

Considering the $2p_{3/2} \rightarrow 4d$ dipole transition with circularly polarized light and a unit difference in magnetic quantum numbers for the initial (m_p) and final (m_d) states given by $\Delta m = m_d - m_p = \pm 1$, $2p_{3/2}$ core electrons tend to be excited into the minority- (majority-) spin 4d states for μ_+ (μ_-) [see inset of Fig. 2(a)]. For the $2p_{3/2} \rightarrow 4s$ transition, $2p_{3/2}$ electrons are prone to be excited into the majority- (minority-) spin channels for μ_+ (μ_-) [Fig. 2(a), inset]. Of interest here is that the XMCD spectrum is expected to represent the difference between the majority- and minority-spin PDOS. It should be noted that the major excitation spin channel of the $2p_{3/2} \rightarrow 4d$ transition is the opposite to that of the $2p_{3/2} \rightarrow 4s$ transition. To examine this idea, we performed

a first-principles band-structure calculation. Figures 2(b) and 2(c) show the calculated total DOS in the majority (upper, red) and minority (lower, blue) spin channels for Co_2MnGe and Co_2MnGa, respectively. We find in the theoretical DOS of Co_2MnGe that a minority spin gap opens with E_F in its center. The shape of the DOS for Co_2MnGa is similar to that of Co_2MnGe, whereas E_F cuts the upper edge of the minority spin valence band and the half-metallicity is therefore destroyed. This supports a rigid band picture where Ge is replaced with Ga. These theoretical DOSs are consistent with previous work [4]. Figure 2(d) [Fig. 2(e)] shows the spin-resolved Ge (Ga) 4*s* and 4*d* PDOS. We recognize that the Ge (Ga) 4*d* PDOS starts to rise above 5 eV and is extended over a wide energy range. In contrast, the Ge (Ga) 4*s* PDOS is relatively small in the corresponding energy region but shows prominent peaks near E_F. Although the Ge (Ga) derived PDOS is about one order of magnitude smaller with respect to the total DOS, a highly spin-splitting feature is recognized even for the Ge (Ga) derived states. This is probably caused by strong hybridization between the Ge (Ga) 4*s*/4*d* and Co/Mn 3*d* orbitals.

The matrix element for the transition from one atomic state (nlm) to another atomic state $(n'l'm')$ is given as follows:

$$\langle \psi_{n'l'm'} | \boldsymbol{\varepsilon} \cdot \boldsymbol{r} | \psi_{nlm} \rangle$$
$$= \mp \sqrt{\frac{4\pi}{3}} \int_0^\infty R^*_{n'l'} R_{nl} r^3 dr \, \langle Y_{l'm'}(\theta,\phi) | Y_{1\pm1}(\theta,\phi) | Y_{lm}(\theta,\phi) \rangle ,$$

where $\psi_{nlm}(r) = R_{nl}(r) Y_{lm}(\theta,\phi)$ and $\psi_{n'l'm'}(r) = R_{n'l'}(r) Y_{l'm'}(\theta,\phi)$ are hydrogen-like atomic wave functions composed of radial functions and spherical harmonic functions represented in spherical polar coordinates. The dipole operator is expressed by $\boldsymbol{\varepsilon} \cdot \boldsymbol{r} = \mp\sqrt{4\pi/3} r Y_{1\pm1}$ with a unit vector $\boldsymbol{\varepsilon} = 1/\sqrt{2}(1, \pm i, 0)$. Here the sign $\pm$ distinguishes the left and right circular photon polarizations with respect to the magnetization direction in the solid. To simulate the XAS and XMCD spectra with the calculated PDOS, the sum over the spectral weights from $2p_{3/2} \rightarrow 4s$ and $2p_{3/2} \rightarrow 4d$ needs to be considered. To this end, we estimated the radial part of the wave function in the transition probabilities, which led to $|\int_0^\infty R^*_{4d} R_{2p} r^3 dr|^2 : |\int_0^\infty R^*_{4s} R_{2p} r^3 dr|^2 = (2\sqrt{5})^2 : 1$. In essence, the radial part of the $2p_{3/2} \rightarrow 4d$ transition probability is 20 times larger than that for the $2p_{3/2} \rightarrow 4s$ transition. The coefficients of absorption and the XMCD are generated as follows by implementing the integrations of spherical harmonics part shown above:

$$\mu_- \propto 20\left(5D^d_{\rm maj} + 3D^d_{\rm min}\right) + D^s_{\rm maj} + 3D^s_{\rm min}, \quad (1)$$

$$\mu_+ \propto 20\left(3D^d_{\rm maj} + 5D^d_{\rm min}\right) + 3D^s_{\rm maj} + D^s_{\rm min}, \quad (2)$$

$$\mu_- + \mu_+ \propto 40\left(D^d_{\rm maj} + D^d_{\rm min}\right) + D^s_{\rm min} + D^s_{\rm maj}, \quad (3)$$

$$\mu_- - \mu_+ \propto 20\left(D^d_{\rm maj} - D^d_{\rm min}\right) + D^s_{\rm min} - D^s_{\rm maj}. \quad (4)$$

Here D^α_β ($\alpha = s, d$, $\beta =$ maj, min) represents the partial density of states of 4*s* or 4*d* orbital in majority- or minority-spin channel. We now compare the calculated Ge 4*d* PDOS with the experimental L_3 edge spectrum [see the upper part of Fig. 3(a)]. Here the horizontal axis represents the energy above E_F and the theoretical Ge 4*d* majority and minority

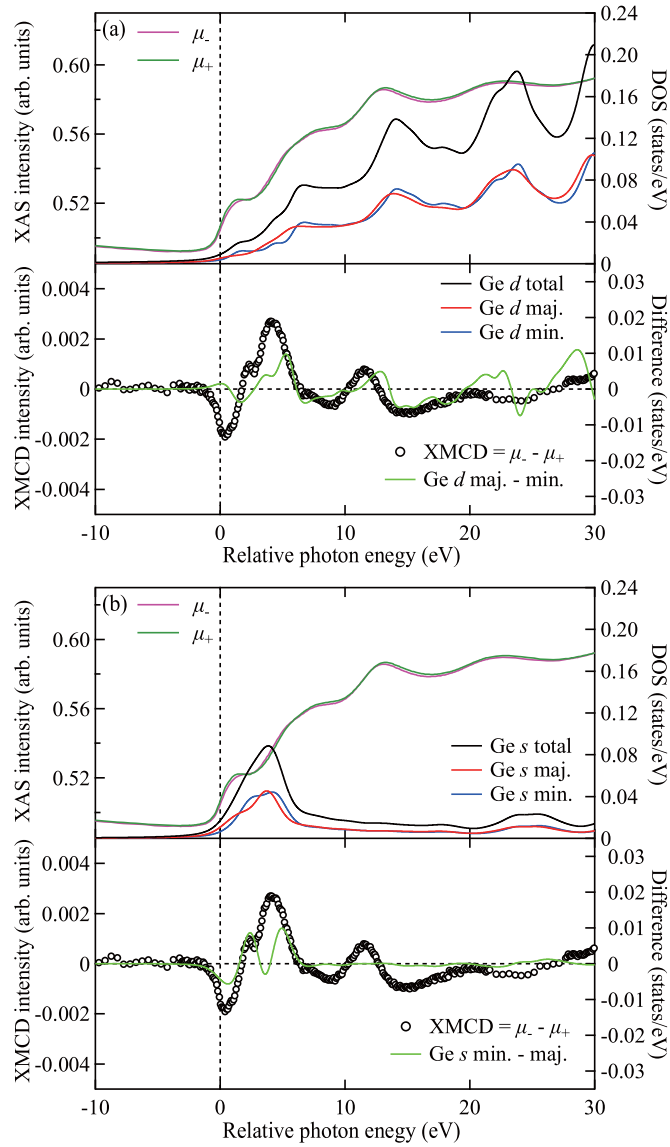

FIG. 3. Calculated total and majority- and minority-spin Ge PDOS for 4*d* (a) and 4*s* (b) convoluted with the Voigt function (upper) and the difference between majority and minority spin DOS (lower) for comparison (see text for details) together with the experimental Ge $L_{2,3}$ edge absorption spectra μ_- (pink), μ_+, and XMCD spectrum (open circles).

PDOS are convoluted with the Voigt function, where both lifetime broadening and energy resolution are taken into account. We see that to some extent the XAS spectral line shape agrees with the shape of the Ge 4*d* PDOS. Near the absorption edge [the A_3 shoulder of Fig. 1(a)], μ_+ is larger than μ_-. At higher energy [B_3–D_3 regions of Fig. 1(a)], the spectral weight of μ_- is located at lower energy than that of μ_+, which results in a positive-to-negative sign change in the XMCD spectrum with increasing incident photon energy. This indicates an exchange-split Ge 4*d* DOS for which the majority part is located at lower energy than the minority part. The lower part of Fig. 3(a) shows the L_3 XMCD spectrum together with the difference between the Ge 4*d* majority and minority DOSs. We claim that the shape of the XMCD spectrum coincides with the difference in the Ge 4*d* PDOS at high energies.

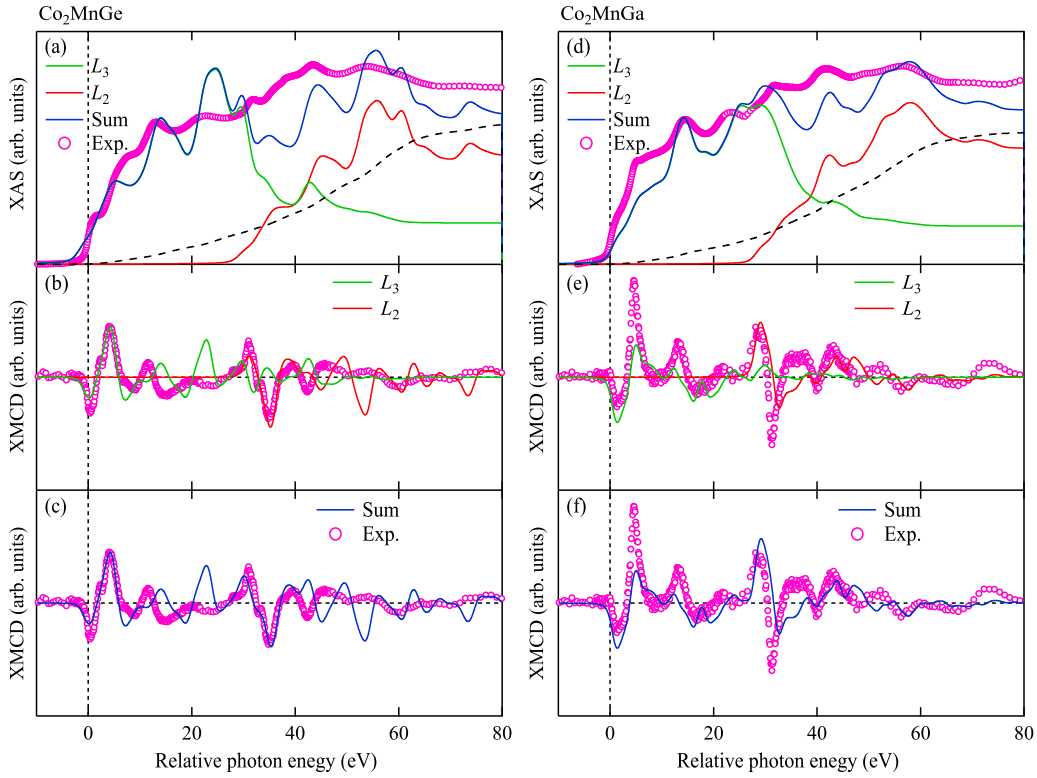

FIG. 4. Computed XAS [(a) and (d)] and XMCD [(b), (c), (e), and (f)] spectra using Eqs. (5) at L_3 (green), L_2 (red), and sum (blue) together with experimental Ge and Ga $L_{2,3}$ edge absorption spectra (pink circle) for Co_2MnGe and Co_2MnGa, respectively.

However, the signs in the Ge 4*d* PDOS and the XMCD results are opposite near E_F. This discrepancy may arise from the absence of the Ge 4*s* PDOS. In the following, we consider the effect of the Ge 4*s* PDOS.

We find that the calculated 4*s* PDOS shows a peak only near E_F, which may correspond to the A_3 shoulder in the experimental XAS spectrum [see Fig. 1(a) and the upper panel of Fig. 3(b)]. The difference between the majority and minority-spin Ge 4*s* PDOSs shows a negative sign near E_F and exhibits two maxima at the higher energy [green line in the lower panel of Fig. 3(b)]. However, no appreciable oscillation appears in the energy region above 10 eV in sharp contrast to the experimental result.

From Eqs. (1)–(4), we find that the contribution of the *s* state is generally small at the $L_{2,3}$ absorption edge. Surprisingly, however, the difference in Ge 4*s* PDOS is in good agreement with the XMCD results [Fig. 3(b)]. These results indicate that the experimental XAS and XMCD spectra, particularly near the absorption edge, cannot be explained only with the theoretical PDOS as long as the atomic wave function is considered for the transition probability.

With this failure in the above-mentioned argument concerning the optical transition probability obtained from the hydrogen-like atomic wave functions, we calculated the XAS and XMCD spectra based on Fermi's golden rule by taking Bloch wave functions into account as described below:

$$\mu_j^{\lambda}(\omega) = \sum_{n\mathbf{k}} |\langle \psi_{n\mathbf{k}} | \mathcal{J}_\lambda | \psi_j \rangle|^2 \delta(E_{n\mathbf{k}} - E_j - \hbar\omega), \qquad (5)$$

where $\hbar\omega$ represents the energy of the photon, λ denotes its polarization, and $\mathcal{J}_\lambda = -e\alpha\mathbf{a}_\lambda$ represents the dipole operator for the electron-photon interaction, where α denotes the Dirac matrices and $\mathbf{a}_\lambda$ denotes the associated λ polarization unit vector of the photon vector potential $a_\pm = (1/\sqrt{2})(1, \pm i, 0)$. The coefficient of absorption μ for incident x-rays is determined by the probability for electron transitions from an initial core state (with wave function ψ_j and energy E_j) to a final unoccupied state (with Bloch wave functions $\psi_{n\mathbf{k}}$ and energies $E_{n\mathbf{k}}$).

To compare the theoretical x-ray isotropic absorption $L_{2,3}$ spectra directly with the experimental spectra, we considered the background intensity caused by different kinds of inelastic scattering of the electron promoted to the conduction band above the E_F via x-ray absorption. To calculate the background spectra, we used the model proposed by Richtmyer *et al.* [39]. The coefficient of absorption for the background intensity ($\mu_{\rm bg}$) is given as

$$\mu_{\rm bg}(\omega) = \frac{C\Gamma_c}{2\pi} \int_{E_{cf_0}}^{\infty} \frac{dE_{cf}}{(\Gamma_c/2)^2 + (\hbar\omega - E_{cf})^2}, \qquad (6)$$

where $E_{cf} = E_c - E_f$, E_c and Γ_c denote the energy and the lifetime broadening of the core hole, E_f denotes the energy of an empty continuum level, E_{f_0} the energy of the lowest unoccupied continuum level, and C a normalization constant, which in this paper has been used as an adjustable parameter. Figure 4(a) shows the calculated Ge L_3 (green) and L_2 (red) edge spectra. The sum of the spectra including the background is also shown to compare with the experimental spectrum (blue). We also show the calculated XMCD spectra at L_3 (green) and L_2 (red) edges [Fig. 4(b)] and their sum (blue) [Fig. 4(c)]. We see an excellent agreement between

theoretical and experimental XMCD spectra, particularly at low energies below 15 eV. We recognize some discrepancies such as a stronger XMCD around $E = 20$ and 53 eV and several energy deviations in the oscillating features above $E = 15$ eV that may come from a possible correlation effect and/or a core hole effect that are not taken into account in the calculation. Nevertheless, we still see an overall agreement between experimental and theoretical spectra. The theoretical spectra of Co_2MnGa also reasonably explain the experimental spectra. Moreover, the theoretical XMCD spectra reproduce the energy difference of these alloys, where the first negative and positive peak positions of Ga are higher than those of Ge. We suggest that it arises because of the difference in the number of valence electrons in these alloys. It also correlates with the circumstance that E_F is located at the lower edge of the minority-spin gap for Co_2MnGa in contrast to Co_2MnGe for which E_F is inside the minority-spin gap.

IV. CONCLUSION

In summary, we performed XAS and XMCD spectroscopy at the Ge and Ga $L_{2,3}$ absorption edges on thin films of full-Heusler alloys of both Co_2MnGe and Co_2MnGa. The observed complex spectral features were compared with the theoretical PDOS of Ge and Ga sites. We found that the Ge (Ga) $L_{2,3}$ XMCD spectrum can be explained qualitatively by the difference between the spin-split majority and minority PDOSs of the Ge 4*d* and 4*s* states. The fully computed XAS and XMCD spectra based on Fermi's golden rule reproduced the experimental XMCD features well, particularly near the Fermi edge. Our finding suggests a means to exploit this method as an experimental tool not only to reveal the spin-split PDOS above E_F through nonmagnetic sites but also for feeding back in computations designing materials with much improved functionalities. Though our experimental results mostly reflect the bulk electronic states, this experimental method can be possibly extended for further application to magnetic-nonmagnetic multilayer systems to scrutinize interface electronic states. It is expected, by performing the measurement with variable temperature, this method that probes spin-dependent electronic states provides us with complementary information of occupied electronic states that can be accessed by spin-resolved photoelectron spectroscopy, and can finally overcome the temperature driven decrease of TMR and GMR.

ACKNOWLEDGMENTS

This work was supported by JSPS KAKENHI (Grants No. 17H06152 and No. 18H03683). The XAS and XMCD measurements were performed at BL23SU of SPring-8 (Proposal No. 2018B3842) under the Shared Use Program of JAEA Facilities (Proposal No. 2018B-E24) with the approval of the Nanotechnology Platform project supported by MEXT, Japan (Proposal No. A-18-AE-0042). Y.S. was financially supported by PRESTO from the Japan Science and Technology Agency (No. JPMJPR17R5). T.Y. and K.S. were financially supported by Grants-in-Aid for JSPS Fellows No. 18J22309 and No. 19J00858, respectively.

[1] M. Julliere, Phys. Lett. A **54**, 225 (1975).
[2] J. Kübler, A. R. Williams, and C. B. Sommers, Phys. Rev. B **28**, 1745 (1983).
[3] S. Ishida, S. Fujii, S. Kashiwagi, and S. Asano, J. Phys. Soc. Jpn. **64**, 2152 (1995).
[4] I. Galanakis, P. H. Dederichs, and N. Papanikolaou, Phys. Rev. B **66**, 174429 (2002).
[5] Y. Sakuraba, M. Hattori, M. Oogane, Y. Ando, H. Kato, A. Sakuma, T. Miyazaki, and H. Kubota, Appl. Phys. Lett. **88**, 192508 (2006).
[6] S. Tsunegi, Y. Sakuraba, M. Oogane, K. Takanashi, and Y. Ando, Appl. Phys. Lett. **93**, 112506 (2008).
[7] T. Taira, T. Ishikawa, N. Itabashi, K. ichi Matsuda, T. Uemura, and M. Yamamoto, J. Phys. D **42**, 084015 (2009).
[8] T. Iwase, Y. Sakuraba, S. Bosu, K. Saito, S. Mitani, and K. Takanashi, Appl. Phys. Exp. **2**, 063003 (2009).
[9] M. J. Carey, S. Maat, S. Chandrashekariaih, J. A. Katine, W. Chen, B. York, and J. R. Childress, J. Appl. Phys. **109**, 093912 (2011).
[10] Y. Sakuraba, K. Izumi, T. Iwase, S. Bosu, K. Saito, K. Takanashi, Y. Miura, K. Futatsukawa, K. Abe, and M. Shirai, Phys. Rev. B **82**, 094444 (2010).
[11] H.-x. Liu, Y. Honda, T. Taira, K.-i. Matsuda, M. Arita, T. Uemura, and M. Yamamoto, Appl. Phys. Lett. **101**, 132418 (2012).
[12] K. Moges, Y. Honda, H.-x. Liu, T. Uemura, M. Yamamoto, Y. Miura, and M. Shirai, Phys. Rev. B **93**, 134403 (2016).
[13] M. Jourdan, J. Minár, J. Braun, A. Kronenberg, S. Chadov, B. Balke, A. Gloskovskii, M. Kolbe, H. J. Elmers, G. Schönhense, H. Ebert, C. Felser, and M. Kläui, Nat. Commun. **5**, 3974 (2014).
[14] R. Fetzer, B. Stadtmüller, Y. Ohdaira, H. Naganuma, M. Oogane, Y. Ando, T. Taira, T. Uemura, M. Yamamoto, M. Aeschlimann, and M. Cinchetti, Sci. Rep. **5**, 8537 (2015).
[15] K. Miyamoto, A. Kimura, Y. Miura, M. Shirai, M. Ye, Y. Cui, K. Shimada, H. Namatame, M. Taniguchi, Y. Takeda, Y. Saitoh, E. Ikenaga, S. Ueda, K. Kobayashi, and T. Kanomata, Phys. Rev. B **79**, 100405(R) (2009).
[16] D. Brown, M. D. Crapper, K. H. Bedwell, M. T. Butterfield, S. J. Guilfoyle, A. E. R. Malins, and M. Petty, Phys. Rev. B **57**, 1563 (1998).
[17] S. Ouardi, G. H. Fecher, B. Balke, A. Beleanu, X. Kozina, G. Stryganyuk, C. Felser, W. Klöß, H. Schrader, F. Bernardi, J. Morais, E. Ikenaga, Y. Yamashita, S. Ueda, and K. Kobayashi, Phys. Rev. B **84**, 155122 (2011).
[18] X. Kozina, J. Karel, S. Ouardi, S. Chadov, G. H. Fecher, C. Felser, G. Stryganyuk, B. Balke, T. Ishikawa, T. Uemura, M. Yamamoto, E. Ikenaga, S. Ueda, and K. Kobayashi, Phys. Rev. B **89**, 125116 (2014).
[19] M. Baral, S. Banik, A. Chakrabarti, D. Phase, and T. Ganguli, J. Alloys Compd. **645**, 112 (2015).
[20] T. Kono, M. Kakoki, T. Yoshikawa, X. Wang, K. Sumida, K. Miyamoto, T. Muro, Y. Takeda, Y. Saitoh, K. Goto, Y. Sakuraba, K. Hono, and A. Kimura, Phys. Rev. B **100**, 165120 (2019).

[21] M. Kallmayer, P. Klaer, H. Schneider, E. Arbelo Jorge, C. Herbort, G. Jakob, M. Jourdan, and H. J. Elmers, Phys. Rev. B **80**, 020406(R) (2009).
[22] P. Klaer, M. Kallmayer, C. G. F. Blum, T. Graf, J. Barth, B. Balke, G. H. Fecher, C. Felser, and H. J. Elmers, Phys. Rev. B **80**, 144405 (2009).
[23] J. Stöhr, J. Magn. Magn. Mater. **200**, 470 (1999).
[24] H. Ebert, Rep. Prog. Phys. **59**, 1665 (1996).
[25] V. Antonov, D. Kukusta, A. Shpak, and A. Yaresko, Condens. Matter Phys. **11**, 627 (2008).
[26] F. M. F. de Groot, J. C. Fuggle, B. T. Thole, and G. A. Sawatzky, Phys. Rev. B **42**, 5459 (1990).
[27] N. D. Telling, P. S. Keatley, G. van der Laan, R. J. Hicken, E. Arenholz, Y. Sakuraba, M. Oogane, Y. Ando, K. Takanashi, A. Sakuma, and T. Miyazaki, Phys. Rev. B **78**, 184438 (2008).
[28] Y. Saitoh, Y. Fukuda, Y. Takeda, H. Yamagami, S. Takahashi, Y. Asano, T. Hara, K. Shirasawa, M. Takeuchi, T. Tanaka, and H. Kitamura, J. Synchrotron Radiat. **19**, 388 (2012).
[29] R. Nakajima, J. Stöhr, and Y. U. Idzerda, Phys. Rev. B **59**, 6421 (1999).
[30] P. Blaha, K. Schwarz, F. Tran, R. Laskowski, G. K. H. Madsen, and L. D. Marks, J. Chem. Phys. **152**, 074101 (2020).
[31] O. K. Andersen, Phys. Rev. B **12**, 3060 (1975).
[32] V. V. Nemoshkalenko, A. E. Krasovskii, V. N. Antonov, V. N. Antonov, U. Fleck, H. Wonn, and P. Ziesche, Phys. Status Solidi (b) **120**, 283 (1983).
[33] J. P. Perdew, K. Burke, and M. Ernzerhof, Phys. Rev. Lett. **77**, 3865 (1996).
[34] A. Manea, O. Monnereau, R. Notonier, F. Guinneton, C. Logofatu, L. Tortet, A. Garnier, M. Mitrea, C. Negrila, W. Branford, and C. Grigorescu, J. Cryst. Growth **275**, e1787 (2005).
[35] V. N. Antonov, B. N. Harmon, and A. N. Yaresko, Phys. Rev. B **63**, 205112 (2001).
[36] V. N. Antonov, B. N. Harmon, and A. N. Yaresko, Phys. Rev. B **66**, 165208 (2002).
[37] V. N. Antonov, B. N. Harmon, and A. N. Yaresko, Phys. Rev. B **66**, 165209 (2002).
[38] V. N. Antonov, B. N. Harmon, O. V. Andryushchenko, L. V. Bekenev, and A. N. Yaresko, Low Temp. Phys. **30**, 305 (2004).
[39] F. K. Richtmyer, S. W. Barnes, and E. Ramberg, Phys. Rev. **46**, 843 (1934).